T2R2 東京科学大学 リサーチリポジトリ
Science Tokyo Research Repository

論文 / 著書情報
Article / Book Information

Title	Valence band offsets at zinc-blende heterointerfaces with misfit dislocations: A first-principles study
Authors	Yoyo Hinuma, Fumiyasu Oba, Isao Tanaka
Citation	Physical Review B, vol. 88, , pp. 075319
Pub. date	2013, 8
Copyright	(c) 2013 American Physical Society
DOI	http://dx.doi.org/10.1103/PhysRevB.88.075319

Powered by T2R2 (Science Tokyo Research Repository)

Valence band offsets at zinc-blende heterointerfaces with misfit dislocations: A first-principles study

Yoyo Hinuma,[1,*] Fumiyasu Oba,[1,2,†] and Isao Tanaka[1,3]

[1]*Department of Materials Science and Engineering, Kyoto University, Kyoto 606-8501, Japan*

[2]*Materials Research Center for Element Strategy, Tokyo Institute of Technology, Yokohama 226-8503, Japan*

[3]*Nanostructures Research Laboratory, Japan Fine Ceramics Center, Nagoya 456-8587, Japan*

(Received 12 July 2013; published 28 August 2013)

The electronic states induced by misfit dislocations at zincblende CdTe/CdS, CdS/ZnS, and InP/GaP heterointerfaces and their impacts on the valence band offsets are investigated using first-principles calculations. The (100) and (110) heterointerfaces including perfect edge dislocations with a Burgers vector of $\frac{a}{2}[1\bar{1}0]$ and a line vector of [001] are considered for each system. Two types of dislocation core structures are found: The "closed" core has four-membered rings only and contains threefold and fivefold coordinated cations, whereas the "open" core has ten-membered rings that involve threefold coordinated atoms. The closed core forms at the (110) interfaces and is energetically more favorable than the open core. The characteristics of dislocation-induced electronic states are heavily dependent on the system and core structure, but all have localized states in the valence and conduction bands. The localized states in the valence band mostly have anion-orbital characteristics, whereas those in the conduction band mainly have cation-orbital characteristics. Some, but not all, dislocation cores also induce electronic states in the gap between the higher of the valence band maxima and the lower of the conduction band minima in the two phases that constitute the interface. The explicit treatment of misfit dislocations changes the valence band offset between the regions at a distance of ∼1 nm or more from the heterointerface by typically ∼0.1 eV.

DOI: 10.1103/PhysRevB.88.075319 PACS number(s): 73.20.−r, 68.35.bg, 61.72.Lk

I. INTRODUCTION

Misfit dislocations at semicoherent heterointerfaces inarguably affect the performance of electronic and optoelectronic devices and photovoltaic cells using semiconductor and/or insulator heterostructures. Misfit dislocations are introduced to release the strain associated with the lattice mismatch between the layers of structurally similar crystals when the thickness of at least one layer exceeds the critical thickness,[1] which can result in the formation of in-gap electronic states that act as carrier traps and also affect the valence and conduction band offsets. In the zincblende structure that many semiconductors take, one common dislocation experimentally observed is the glissile 60° dislocation with a Burgers vector of $\mathbf{b} = \frac{a}{2}[10\bar{1}]$ on the (111) plane. Two of these 60° dislocations can form the sessile 90° (pure edge) Lomer dislocation with $\mathbf{b} = \frac{a}{2}[110]$[2–4] through the reaction $\frac{a}{2}[10\bar{1}](111) + \frac{a}{2}[011](\bar{1}\bar{1}1) = \frac{a}{2}[110](001)$.[2] Another experimentally reported 90° dislocation is located on the (110) plane and has $\mathbf{b} = \frac{a}{2}[1\bar{1}0]$.[5–8] In a (001)-oriented interface, the Burgers vector of this dislocation is inclined at 45° to the interfacial plane.

Ultraviolet and x-ray photoelectron spectroscopy is often used to obtain the valence band offset. The reported values, however, differ from each other because band offsets are strongly dependent on the orientation, atomic configuration, and chemical composition of the interface. For example, the experimentally obtained valence band offset of CdTe/CdS with a lattice misfit of ∼10%[9,10] differs by ∼0.3 eV depending on the preparation method.[11–13] The experimental valence band offset of $CuInSe_2$/CdS, which has a lattice misfit as small as 0.4%,[14,15] varies by about 0.8 eV[16–21] partly because an interlayer consisting of ordered vacancy compounds[17] may or may not exist. Theoretical approaches are effective in obtaining the offset values for ideal interfaces and in elucidating the contributions of additional effects such as point defects and dislocations. A typical approach is the evaluation of strained and unstrained, or natural, band offsets via first-principles calculations using coherent, or lattice-matched, interface models.[22–25] The effects of the lattice relaxation on the natural band offset are considered via deformation potential[26–29] or surface calculations,[25,30] neglecting the presence of misfit dislocations at semicoherent interfaces. Although rather limited, there are first-principles studies that explicitly treat misfit dislocations. Examples include calculations of an InAs/GaAs (110) interface with an edge dislocation with $\mathbf{b} = \frac{a}{2}[1\bar{1}0]$ and a line vector of $\boldsymbol{\xi} = [001]$, in which a thin slab of a substrate material coated with a few layers of a secondary material was employed.[31,32] The SiC/Si (001) interface involving edge dislocations with $\mathbf{b} = \frac{a}{2}[1\bar{1}0]$ and $\boldsymbol{\xi} = [110]$ has been investigated using a vacuum-separated slab containing the semicoherent heterointerface.[33] The atomistic and electronic structures as well as energetics of misfit dislocations have been discussed in these studies but their effects on the band offsets have not been reported.

We investigate the valence band offsets at CdTe/CdS, CdS/ZnS, and InP/GaP semicoherent interfaces using first-principles calculations in the present study. A one-dimensional array of misfit dislocations at the (110) and (100) heterointerfaces is modeled using a supercell that includes a pair of heterointerfaces. The atomic configurations of the dislocation cores and the induced electronic states are discussed in addition to the effects of the dislocations on the valence band offsets.

II. METHODOLOGY

The calculations were performed on the basis of density functional theory[34,35] using the projector-augmented wave (PAW) method[36] and the Perdew-Burke-Ernzerhof generalized gradient approximation (GGA) functional[37,38] as implemented in the Vienna *Ab initio* Simulation Package (VASP).[39–41] A

 ©2013 American Physical Society

plane-wave cutoff energy of 350 eV and PAW datasets with the following valence electronic states and radial cutoffs[41] were used: $4d$, $5s$, $5p$ and 1.2 Å for Cd; $3d$, $4s$, $4p$ and 1.2 Å for Zn; $4s$, $4p$ and 1.4 Å for Ga; $5s$, $5p$ and 1.6 Å for In; $3s$, $3p$ and 1.0 Å for P and S; and $5s$, $5p$ and 1.2 Å for Te. Calculations of interfaces with misfit dislocations were carried out using supercells detailed below with Γ-centered k-point meshes of $1 \times 1 \times 4$. Site-projected electronic densities of states (DOSs) were calculated with k-point meshes of $2 \times 2 \times 16$. The supercell dimensions and internal atomic coordinates were allowed to fully relax.

We use the following interface models under three-dimensional periodic boundary conditions. The ratios of the calculated lattice constants of CdS/CdTe, ZnS/CdS, and GaP/InP are 0.897, 0.919, and 0.922, respectively, which are close to 9/10 (=0.900), 11/12 (=0.917), and 13/14 (=0.929), respectively. Those of the experimental lattice constants are similar, which are 0.898, 0.930, and 0.929, respectively. Actual semicoherent interfaces have two-dimensional dislocation networks with an interdislocation distance determined by these misfits and the Burgers vectors, but it is not feasible to explicitly treat such interfaces in the supercells for first-principles calculations. Therefore, we consider an interface with a one-dimensional array of misfit dislocations. Two phases alternate in the stacking direction of the supercells, with an interface plane of either (110) or (100) and perfect edge dislocations with $\mathbf{b} = \frac{a}{2}[1\bar{1}0]$ and $\boldsymbol{\xi} = [001]$. We use supercells containing 9 and 11 layers for each of the two phases in the (110) interface calculations and 14 and 14 layers each in the (100) interface calculations; convergence has been checked using 13 and 15 layers for (110) and 18 and 18 layers for (100) interface calculations, respectively, and the valence band offset changed by 0.03 eV or less when the number of layers was increased. The cell dimension is taken as short as possible in the [001] direction parallel to the dislocation line, which approximately corresponds to the average of the lattice constants of the two phases. The number of atoms per supercell is different in the direction perpendicular to the dislocation line and stacking directions, and the supercell dimension in this direction is initially determined by the lattice misfit and the Burgers vector, as mentioned above.

Figure 1 shows the relaxed structures of CdS/ZnS supercells with (110) and (100) interfaces. The interdislocation distance after relaxation amounts to 46.2 and 66.6 Å for the (110) and (100) interface models shown, respectively. The number of atoms in the width direction ([$\bar{1}$10] in Fig. 1(a) and [010] in Fig. 1(b)) is fewer in CdS (red and green balls) at the center compared to that in ZnS (blue and green balls) at the top and bottom. The total number of atoms in the supercell amounts to 462 and 648 in Figs. 1(a) and 1(b), respectively. We found that the changes in band offsets are within 0.01 eV when relative positions of the dislocations cores are shifted in the direction parallel to the Burgers vector at the (110) interfaces, and therefore the band offsets do not significantly depend on the relative position of the dislocation cores. Figure 2 shows the four types of initial atomic configurations

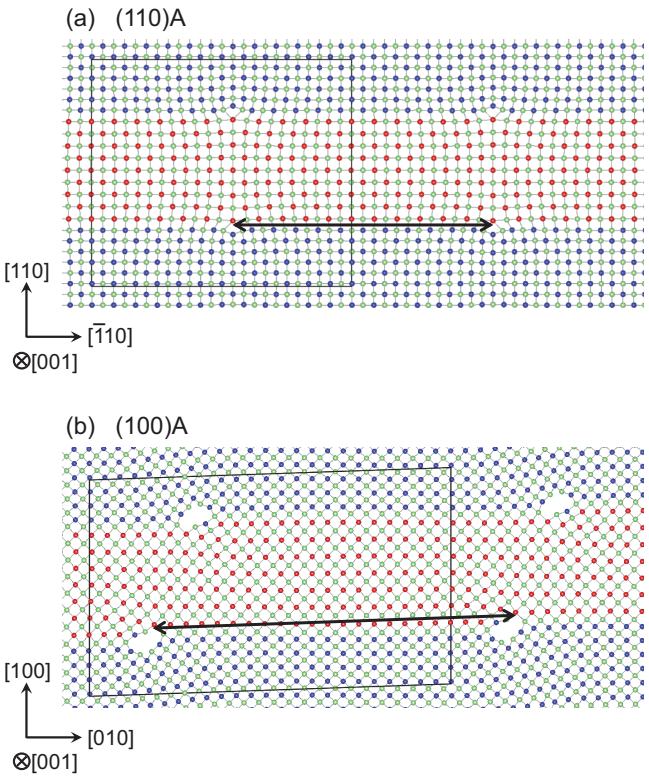

FIG. 1. (Color online) Structure of CdS/ZnS interface supercells containing misfit dislocations, (a) (110) and (b) (100) interfaces, both of which have perfect edge dislocations with a Burgers vector of $\frac{a}{2}[1\bar{1}0]$ and a line vector of [001]. The black frame represents the supercell, and dislocations are separated by the distance indicated by the arrows [46.2 Å and 66.6 Å for the (110) and (100) interfaces shown, respectively]. Red, blue, and green circles denote Cd, Zn, and S atoms, respectively.

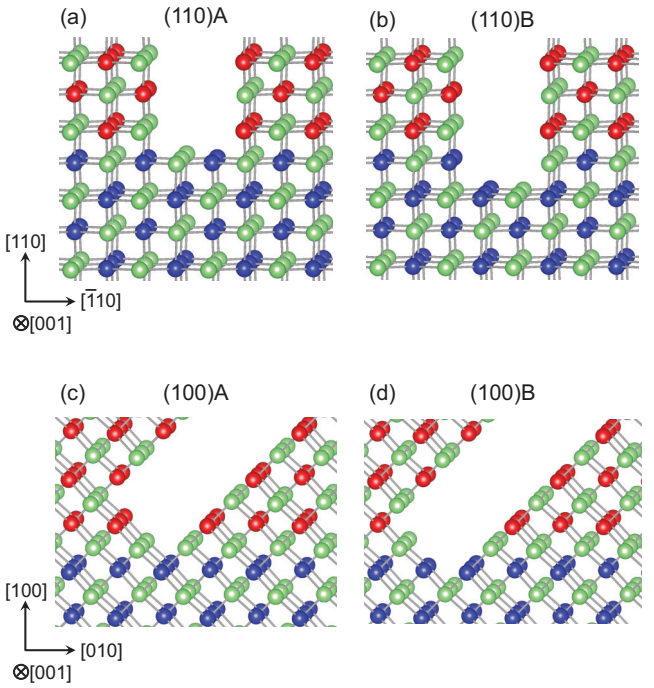

FIG. 2. (Color online) Four types of initial atomic configurations around dislocations at CdS/ZnS (110) and (100) interfaces. Red, blue, and green circles denote Cd, Zn, and S atoms, respectively.

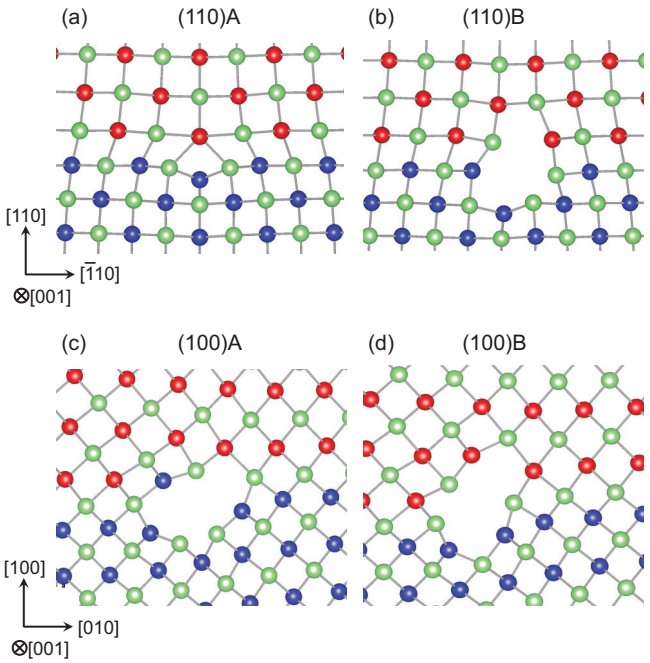

FIG. 3. (Color online) Relaxed dislocation core structures at CdS/ZnS (110) and (100) interfaces. Red, blue, and green circles denote Cd, Zn, and S atoms, respectively.

around the dislocations, which lead to different dislocation core structures. Two types of the configurations that differ by the number of removed atoms (A and B) are investigated for each of the (110) and (100) interfaces. The CdTe/CdS, CdS/ZnS, and InP/GaP systems considered in this work all have a common cation or anion and, as shown later, have similar atomic configurations at dislocation cores.

III. RESULTS AND DISCUSSION

A. Atomic configurations and relative stability of dislocation cores

The relaxed atomic configurations around dislocation cores at the CdS/ZnS interfaces are shown in Fig. 3. There are two types of dislocation cores. The first is the "closed" core with four-membered rings only in the [001] projection and contains threefold coordinated and fivefold coordinated atoms and is denoted as the (110)A core [Fig. 3(a)]. This core structure is similar to those reported for an InAs/GaAs (110) interface.[31,32] The second is the "open" core with ten-membered rings and threefold coordinated atoms but no fivefold coordinated atoms, which represents the remaining three core types, denoted as (110)B, (100)A, or (100)B [Figs. 3(b)–3(d)]. Similar core structures are obtained for the other two systems; however, the InP/GaP (100)B core is a somewhat crushed but still open core that is slightly different from CdTe/CdS and CdS/ZnS.

The relative stability of the two types of cores, A and B, can be discussed using the energy difference per supercell, which is given as

$$\Delta E = E_{\mathrm{A}} - E_{\mathrm{B}} - \sum_i \Delta n_i E_i, \qquad (1)$$

where E_{A} and E_{B} are the total energies of the supercells containing dislocation cores A and B, respectively, Δn_i is the difference in the number of formula units for the constituent compound i between cores A and B, and E_i is the total energy of the compound i per formula unit. Taking the dislocations at the CdS/ZnS interfaces shown in Figs. 2 and 3 as an example, $\Delta n_{\mathrm{ZnS}} = 2$ and $\Delta n_{\mathrm{CdS}} = 2$ for the (110) and (100) interfaces, respectively. The energy difference per unit dislocation length is obtained by dividing the quantity in Eq. (1) by the dislocation length, that is, twice the relaxed supercell dimension in the dislocation line direction or approximately twice the average of the lattice constants of the two constituent phases; the factor of two appears because there are two dislocations per supercell. Exactly what should be used as E_i is a nontrivial question because the two phases in the supercells are strained along the directions parallel to the dislocation line so that the in-plane lattice constants are the same. Here, we discuss relative energies per supercell and use the unstrained bulk energy of ZnS or CdS, thus neglecting the effects of such strain. The relative stability of the dislocation cores in CdTe/CdS and InP/GaP systems is evaluated similarly. The energy difference per supercell between cores (110)A and (110)B is -0.88, -0.70, and -1.52 eV for CdTe/CdS, CdS/ZnS, and InP/GaP, respectively, and that between (100)A and (100)B is 0.11, -0.38, and 1.09 eV, respectively. The closed cores have lower energies than the open cores according to the results for the (110) cores, presumably because there are fewer dangling bonds. The energy difference per supercell can change by up to 0.4 eV when the relative positions of the two dislocation cores are shifted by about one-half of the interdislocation distance in the direction parallel to the Burgers vector, but the (110)A core is still more stable than the (110)B core. Open (100)A and (100)B cores in CdTe/CdS and CdS/ZnS, which are similar in atomic arrangements, have similar energies.

Previous high-resolution transmission electron microscopy and scanning transmission electron microscopy studies have revealed that dislocations in semiconductors show multiple core configurations.[3,42,43] Therefore, we consider both closed (110)A and open (110)B cores, despite the energetic preference of the former, and discuss how open and closed cores affect electronic properties hereafter.

B. Electronic states induced by the dislocation

Figure 4 shows the site-projected electronic DOS in the vicinity of the (110)A and (110)B cores in the three systems. Figures 4(a)–4(d) show the atomic configurations of the relaxed cores, and Figs. 4(e)–4(j) give the projected DOS at the atomic sites labeled in Figs. 4(a)–4(d). The dashed lines in Figs. 4(e)–4(j) indicate the higher valence band maximum (HVBM) and the lower conduction band minimum (LCBM), which are the higher of the two valence band maxima (VBM) and the lower of the two conduction band minima (CBM) in bulklike regions far from the interface in the two phases, respectively. The HVBM and LCBM are determined using the VBM and CBM from bulk calculations via reference level alignment between the bulk cells and the bulklike regions in interface supercells, and this procedure follows that of valence band offset evaluation described later.

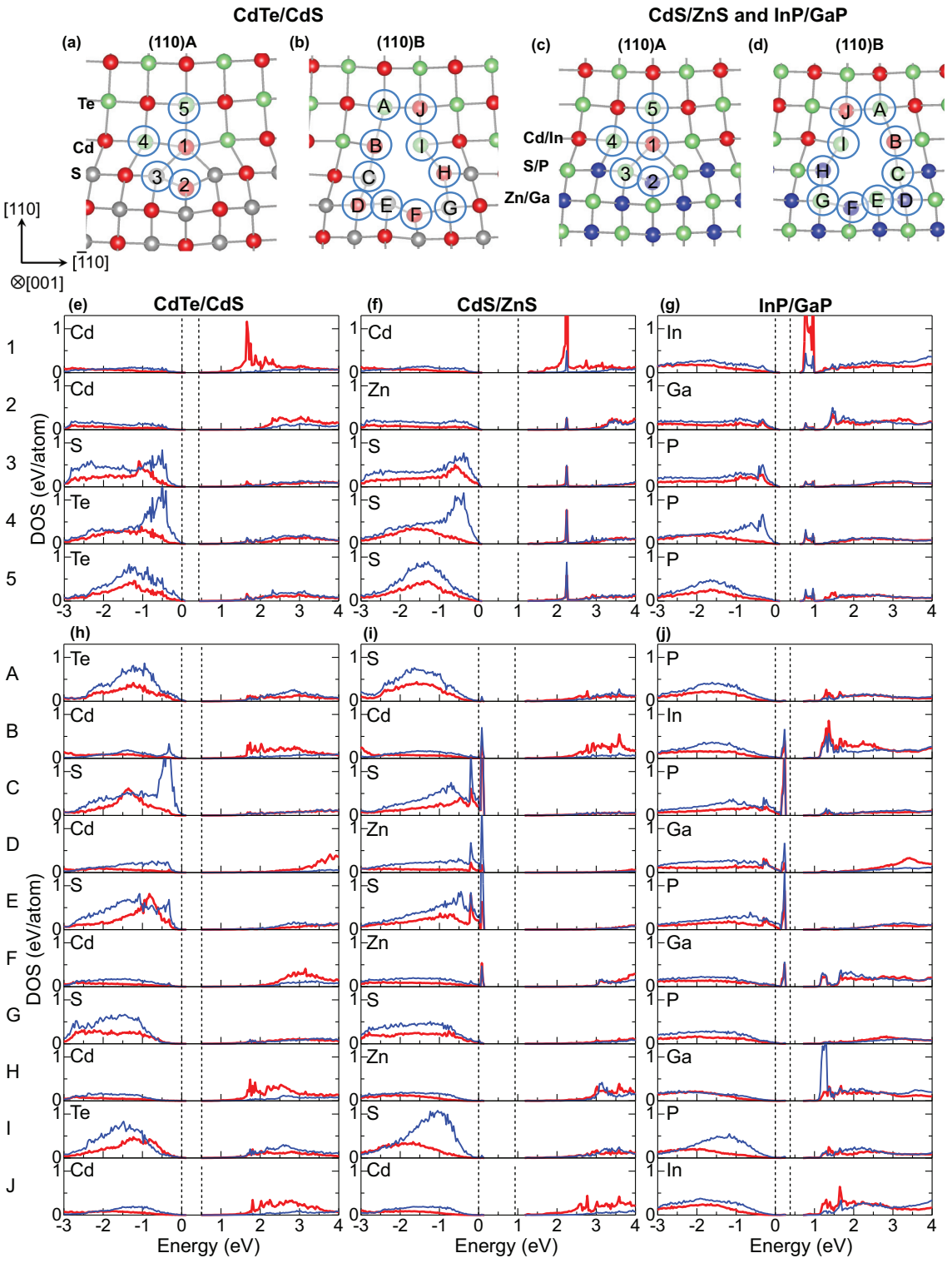

FIG. 4. (Color online) Site-projected electronic DOS in the vicinity of dislocation cores. The DOS at each atomic site indicated in (a)–(d) is presented in (e)–(j). Thick red and thin blue curves show *s* and *p* orbital components, respectively. The dashed lines show the higher VBM and lower CBM of the two phases estimated from bulklike regions far from the interface; the former is taken as the zero of the energy.

We first focus on the (110)A cores [Figs. 4(e)–4(g)]. The fivefold coordinated sites (site 1) are cations in all cases (Cd or In), and there are large peaks localized on the site 1 cations in the conduction band in all three cores. There is a peak at about 1.3 eV above the LCBM both in the CdTe/CdS (110)A core [Fig. 4(e)] and in the CdS/ZnS (110)A core [Fig. 4(f)]. These peaks consist mainly of Cd 5*s* orbitals. On the other hand, there is a double peak at 0.4 and 0.6 eV above the

LCBM in the InP/GaP (110)A core [Fig. 4(g)]. Furthermore, there is a small peak on Ga at site 2 at ∼1.1 eV above the LCBM. The dislocation-induced states in the conduction band involve *s* and *p* orbitals of nearby atoms in the CdS/ZnS (110)A core and, to a lesser extent, in the InP/GaP (110)A core. In addition, there is absolutely no electronic state on and up to ∼0.2 eV above the LCBM for the CdS/ZnS (110)A and InP/GaP (110)A cores in the interface supercells; here, note that the LCBM does not necessarily correspond to the lowest unoccupied level in the interface supercells since the LCBM is determined using the CBM from bulk calculations via reference level alignment, as mentioned above. A similar situation has been observed at the $CuInSe_2$/CdS interface when there are ordered V_{Cu} and In_{Cu} at the interface,[25] implying that this heightening of the conduction band edge arises from existence of specific defects (dislocations). In addition to the localized states in the conduction band, broad dislocation-induced peaks exist in the valence band in all three cores. These states have *p* orbital characteristics of the anions at sites 3 and 4 and are distributed around 0.3 eV below the HVBM. Thus, dislocation cores (110)A induce electronic states within the valence and conduction bands of the constituent phases of the interfaces. However, dislocation-induced states are completely absent in the gap between the HVBM and the LCBM, which is important information when carrier trapping is considered.

We now look at the (110)B cores [Figs. 4(h)–4(j)]. Dislocation-induced states with cation-orbital characteristics are found in the conduction band as in the (110)A cores. One such state is distributed over the B, H, and J sites at ∼1.5 eV above the LCBM and has a Cd 5*s* characteristic for the CdTe/CdS (110)B core [Fig. 4(h)] and also over the B and J sites at ∼1.8 eV above the LCBM for the CdS/ZnS (110)B core [Fig. 4(i)]. There is a distinct dislocation state for the InP/GaP (110)B core [Fig. 4(j)] at ∼1 eV above the LCBM. It is localized primarily on the H site with a Ga 4*p* characteristic, but also involves *s* and *p* states of neighboring cations, that is, In on B and J sites and Ga on the F site. There is no electronic state at or slightly above the LCBM in the CdS/ZnS (110)B and InP/GaP (110)B cores, as in the respective (110)A cores. Furthermore, significant and sharp in-gap dislocation states are recognized directly above the HVBM in CdS/ZnS (110)B and in the middle of the gap in InP/GaP (110)B. These states are localized mainly on the C and E anion sites but also extend over the B, D, and F cation sites, and there is a continuous nonzero distribution of DOS from the valence band into these in-gap states. In the valence band, there are dislocation states mainly consisting of the *p* orbitals of anions at about 0.2 to 0.3 eV below the HVBM in all three (100)B cores, and this trend is similar to that found in the (110)A cores.

In summary, every investigated dislocation core has localized states in the valence and conduction bands. However, the details of the dislocation states, such as the peak position and height in the DOS and the extent of spatial distribution, depend on the shape of the core, in addition to the pair of phases that form the heterointerface. The dislocation states in the conduction band have mainly cation-orbital characteristics, while those in the valence band and the gap between the HVBM and LCBM have mostly anion-orbital characteristics.

C. Valence band offset

Knowledge on the influence of misfit dislocations on the natural band offset is indisputably important when we consider systems with semicoherent interfaces. The valence band offset is evaluated as

$$\Delta\varepsilon_{\mathrm{VBM}}^{\mathrm{A-B}} = \Delta\varepsilon_{\mathrm{VBM-Ref}}^{\mathrm{A}} - \Delta\varepsilon_{\mathrm{VBM-Ref}}^{\mathrm{B}} + \Delta\varepsilon_{\mathrm{Ref}}^{\mathrm{A-B}}. \qquad (2)$$

A calculation using an interface supercell including misfit dislocations is used to obtain the difference between reference levels near the center of slabs of two phases, A and B, $\Delta\varepsilon_{\mathrm{Ref}}^{\mathrm{A-B}} = \varepsilon_{\mathrm{Ref}}^{\mathrm{A}} - \varepsilon_{\mathrm{Ref}}^{\mathrm{B}}$. The reference level is determined by averaging the average electrostatic potential at atomic sites over regions at a distance of ∼8 Å or more from the interface. Unstrained bulk calculations provide the energy difference from the reference level to the VBM for phase A, $\Delta\varepsilon_{\mathrm{VBM-Ref}}^{\mathrm{A}} = \varepsilon_{\mathrm{VBM}}^{\mathrm{A}} - \varepsilon_{\mathrm{Ref}}^{\mathrm{A}}$, and $\Delta\varepsilon_{\mathrm{VBM-Ref}}^{\mathrm{B}}$ can be obtained similarly for phase B. This is based on the assumption that the strain is completely released in the region far from actual interfaces.

Equation (2) is identical to the simplified natural band offset defined in Ref. 25, except that the third term is evaluated using an interface supercell with a one-dimensional array of misfit dislocations in this study. Without explicit treatment of a two-dimensional network of misfit dislocations, at least one of the two phases must be strained because either or both of the in-plane lattice parameters must be the same between two phases in the interface supercell. The two phases have a common lattice parameter in the direction parallel to the dislocation line in the present supercell and, therefore, involve compressive or tensile strains. In addition, a small in-plane strain is left in the direction perpendicular to the dislocation line because of the small difference of the cell dimension in this direction corresponding to the interdislocation distance from that exactly given by the actual misfit (e.g., 0.897 vs 0.900 for CdS/CdTe, as mentioned above) and also because of the full cell optimization in the presence of compressive or tensile strain in the direction along the dislocation line. In principle, corrections for the change in the reference level associated with the strain relief should be considered using deformation potential[26–29] or surface calculations.[25,30] However, such terms are omitted in Eq. (2) because our previous studies found that in-plane strain dependence of the reference level is typically weak enough that carrying out surface calculations to estimate the reference level shift can be a larger source of error as the local dipole moments at the surfaces with different

TABLE I. Natural valence band offsets of CdTe/CdS, CdS/ZnS, and InP/GaP interfaces obtained using supercells with and without misfit dislocations. The values are with respect to CdS for CdTe/CdS, ZnS for CdS/ZnS, and GaP for InP/GaP.

Interface plane	Dislocation core type	Valence band offset (eV) CdTe/CdS	CdS/ZnS	InP/GaP
(110)	None	0.64	−0.01	0.19
	A	0.63	−0.05	0.06
	B	0.55	−0.13	0.00
(100)	None	0.61	−0.12	0.11
	A	0.63	−0.20	0.00
	B	0.52	−0.10	0.08

in-plane lattice parameters cannot completely cancel out.[25,44] The natural band offset evaluated using Eq. (2) and interface supercells without misfit dislocations is found to be almost independent of their in-plane lattice parameters, where the difference of the $CuInSe_2$/ZnS valence band offset is less than 0.05 eV when the in-plane lattice parameters are varied by the lattice misfit of about 7%.[25] Corrections for the relaxation of the in-plane lattice parameters using surface calculations are less than 0.1 eV for the valence band offsets between chalcopyrite $CuInSe_2$, $CuGaSe_2$, $ZnSnP_2$, and $CdSnP_2$ versus zincblende CdS and ZnS.[44]

The valence band offsets obtained using interface supercells involving misfit dislocations are shown in Table I. Values obtained using coherent interface supercells without misfit dislocations are also listed, where the difference in the band offset between the (110) and (100) interfaces is small and at most ∼0.1 eV. Explicit consideration of misfit dislocations changes the band offset by −0.19 to 0.02 eV. Thus, the absolute value of the correction to the band offset is not more than 0.2 eV in the systems considered; if we exclude the energetically less favorable (110)B configurations from the (110) interfaces, the change is only up to ∼0.1 eV.

Among the three pairs of zincblende compounds considered in this work, the CdTe/CdS valence band offset has been studied extensively because of its use in photovoltaic applications, and many experimental offset values are reported. CdS film grown by molecular beam epitaxy on CdTe(110) shows a valence band offset of 0.65 eV according to Niles and Höchst.[11] Al Kuhaimi gave values of 0.67 to 0.7 eV for CdS film evaporated on CdTe film.[12] On the other hand, Fritsche *et al*. reported 0.94 ± 0.05 eV for polycrystalline CdTe film evaporated on CdS film.[13] The calculated value of about 0.6 eV

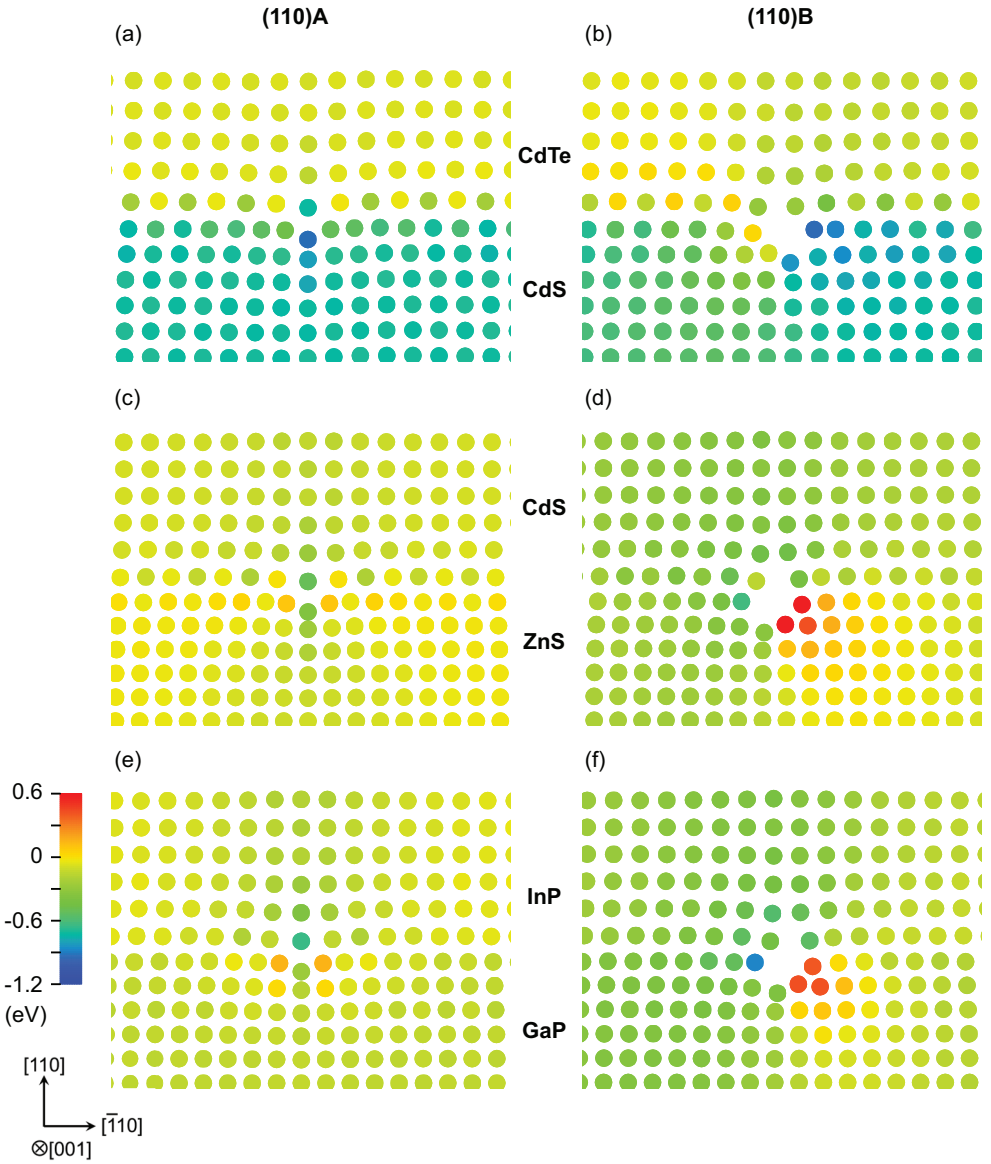

FIG. 5. (Color online) Distributions of average electrostatic potentials at atomic sites in interface supercells with dislocation cores (110)A and (110)B. The atomic sites are represented by circles. The electrostatic potentials are rigidly shifted so that the difference between the upper and lower regions far from the interface (at a distance of ∼8 Å or more) approximately corresponds to the valence band offset.

is in line with the experimental results, although the details of the interfacial structures in the band offset measurements have not been reported and hence direct comparison cannot be made between the calculated and experimental values.

To understand the effect of a dislocation on the valence band offset, the distribution of average electrostatic potentials at atomic sites, which is used to determine the reference level in the offset evaluation, is investigated. Figure 5 shows distributions of average electrostatic potentials at atomic sites in interface supercells with dislocation cores (110)A and (110)B. The electrostatic potentials are rigidly shifted so that the difference between the bulklike regions of the two phases (the upper and lower regions in Fig. 5) approximately corresponds to the valence band offset.

There is a striking contrast between the results for the (110)A and (110)B cores. The perturbation to the electrostatic potential is extremely localized in the (110)A cores and limited to a few atoms near the core, as shown in Figs. 5(a),5(c), and 5(e). Therefore, the difference in the electrostatic potential between the two phases, which corresponds to the valence band offset, is almost uniform except for the immediate vicinity of the dislocation cores. On the other hand, there are two prominent features in the (110)B cores [Figs. 5(b), 5(d), and 5(f)]. One is the presence of a high-value region originating at a pair of anions at the bottom left [Fig. 5(b)] or bottom right [Figs. 5(d) and 5(f)] of the core that extends over a range exceeding 10 Å (several atomic sites). The other feature is a low-value region centered on an extremely low cation at the right [Fig. 5(b)] or left [Figs. 5(d) and 5(f)] of the core, and spreading to a few nearby anions at the top left of the core in Figs. 5(d) and 5(f). The overall results are consistent with the findings from the site-projected DOS in Fig. 4; the atomic sites on which localized states are mainly distributed correspond to the sites with electrostatic potentials significantly dissimilar to those in the bulklike region. Such a difference in the electrostatic potentials is gradually reduced with a distance from the dislocation cores, but the influence prevails even in the bulklike region far from the cores. The natural valence band offsets listed in Table I indicate that the average shift of the electrostatic potential by the presence of misfit dislocations is not significant in the bulklike region, but the local electrostatic potential varies there.

IV. CONCLUSIONS

We have investigated misfit dislocations at (110) and (100) heterointerfaces of zincblende CdTe/CdS, CdS/ZnS, and InP/GaP systems using first-principles calculations. Two types of core structures are found for perfect edge dislocations with $\mathbf{b} = \frac{a}{2}[1\bar{1}0]$ and $\boldsymbol{\xi} = [001]$: the closed core with four-membered rings that contains threefold and fivefold coordinated cations and the open core with ten-membered rings that has threefold coordinated atoms but not fivefold coordinated atoms. The closed core is energetically preferred at the (110) interfaces. Dislocation-induced electronic states strongly depend on the system and core structure, but all systems investigated have dislocation states in the valence and conduction bands. The dislocation states in the valence band tend to be localized on anions, whereas those in the conduction band tend to be localized on cations. Some but not all cores induce in-gap states. The average valence band offset at a distance of $\sim$1 nm or more from the heterointerface typically shows a small change of less than 0.1 eV with the introduction of misfit dislocations into the supercells in all investigated cases.

ACKNOWLEDGMENTS

This work was supported by Grants-in-Aid for Young Scientists (A) (Grant No. 23686089) and Scientific Research on Innovative Areas "Nano Informatics" (Grant No. 25106005) from JSPS and the MEXT Elements Strategy Initiative to Form Core Research Center "Tokodai Institute for Element Strategy (TIES)." Computing resources of ACCMS at Kyoto University were used in this work. The VESTA code[45] was used to draw Figs. 1–4.

*yoyo.hinuma@gmail.com
†oba@cms.mtl.kyoto-u.ac.jp

[1] J. W. Matthews and A. E. Blakeslee, J. Cryst. Growth **27**, 118 (1974).
[2] Y. B. Bolkhovityanov, A. S. Deryabin, A. K. Gutakovskii, and L. V. Sokolov, J. Appl. Phys. **109**, 123519 (2011).
[3] S. Lopatin, S. J. Pennycook, J. Narayan, and G. Duscher, Appl. Phys. Lett. **81**, 2728 (2002).
[4] M. Loubradou, R. Bonnet, and F. R. Chen, Surf. Interface Anal. **30**, 616 (2000).
[5] J. M. Bonar, R. Hull, J. F. Walker, and R. Malik, Appl. Phys. Lett. **60**, 1327 (1992).
[6] M. Albrecht, H. P. Strunk, R. Hull, and J. M. Bonar, Appl. Phys. Lett. **62**, 2206 (1993).
[7] X. Zhang, D. W. Pashley, L. Hart, J. H. Neave, P. N. Fawcett, and B. A. Joyce, J. Cryst. Growth **131**, 300 (1993).
[8] J. G. Belk, J. L. Sudijono, X. M. Zhang, J. H. Neave, T. S. Jones, and B. A. Joyce, Phys. Rev. Lett. **78**, 475 (1997).
[9] R. J. Traill and R. W. Boyle, Am. Mineral. **40**, 555 (1955).
[10] M. G. Williams, R. D. Tomlinson, and M. J. Hampshire, Solid State Commun. **7**, 1831 (1969).
[11] D. W. Niles and H. Höchst, Phys. Rev. B **41**, 12710 (1990).
[12] S. A. Al Kuhaimi, Energy **25**, 731 (2000).
[13] J. Fritsche, T. Schulmeyer, D. Kraft, A. Thissen, A. Klein, and W. Jaegermann, Appl. Phys. Lett. **81**, 2297 (2002).
[14] H. W. Spiess, U. Haeberlen, G. Brandt, A. Räuber, and J. Schneider, Phys. Status Solidi B **62**, 183 (1974).
[15] R. J. Traill and R. W. Boyle, Am. Mineral. **40**, 555 (1955).
[16] Y. Hashimoto, K. Takeuchi, and K. Ito, Appl. Phys. Lett. **67**, 980 (1995).
[17] D. Schmid, M. Ruckh, F. Grunwald, and H. W. Schock, J. Appl. Phys. **73**, 2902 (1993).
[18] T. Löher, W. Jaegermann, and C. Pettenkofer, J. Appl. Phys. **77**, 731 (1995).
[19] D. Schmid, M. Ruckh, and H. W. Schock, Sol. Energy Mater. Sol. Cells **41–42**, 281 (1996).

[20]A. J. Nelson, D. W. Niles, C. R. Schwerdtfeger, S.-H. Wei, A. Zunger, and H. Höchst, J. Electron Spectrosc. Relat. Phenom. **68**, 185 (1994).
[21]A. Klein, T. Löher, Y. Tomm, C. Pettenkofer, and W. Jaegermann, Appl. Phys. Lett. **70**, 1299 (1997).
[22]A. Janotti and C. G. Van de Walle, Phys. Rev. B **75**, 121201 (2007).
[23]Y.-H. Li, A. Walsh, S. Chen, W.-J. Yin, J.-H. Yang, J. Li, J. L. F. Da Silva, X. G. Gong, and S.-H. Wei, Appl. Phys. Lett. **94**, 212109 (2009).
[24]E. S. Kadantsev and P. Hawrylak, Appl. Phys. Lett. **98**, 023108 (2011).
[25]Y. Hinuma, F. Oba, Y. Kumagai, and I. Tanaka, Phys. Rev. B **88**, 035305 (2013).
[26]C. G. Van de Walle and R. M. Martin, Phys. Rev. Lett. **62**, 2028 (1989).
[27]R. Resta, L. Colombo, and S. Baroni, Phys. Rev. B **41**, 12358 (1990).
[28]A. Franceschetti, S.-H. Wei, and A. Zunger, Phys. Rev. B **50**, 17797 (1994).
[29]Y.-H. Li, X. G. Gong, and S.-H. Wei, Appl. Phys. Lett. **88**, 042104 (2006).
[30]S. Lany, J. Osorio-Guillén, and A. Zunger, Phys. Rev. B **75**, 241203 (2007).
[31]N. Oyama, E. Ohta, K. Takeda, K. Shiraishi, and H. Yamaguchi, Surf. Sci. **433–435**, 900 (1999).
[32]R. Choudhury, D. R. Bowler, and M. J. Gillan, J. Phys.: Condens. Matter **20**, 235227 (2008).
[33]L. Pizzagalli, G. Cicero, and A. Catellani, Phys. Rev. B **68**, 195302 (2003).
[34]P. Hohenberg and W. Kohn, Phys. Rev. **136**, B864 (1964).
[35]W. Kohn and L. J. Sham, Phys. Rev. **140**, A1133 (1965).
[36]P. E. Blöchl, Phys. Rev. B **50**, 17953 (1994).
[37]J. P. Perdew, K. Burke, and M. Ernzerhof, Phys. Rev. Lett. **77**, 3865 (1996).
[38]J. P. Perdew, K. Burke, and M. Ernzerhof, Phys. Rev. Lett. **78**, 1396 (1997).
[39]G. Kresse and J. Hafner, Phys. Rev. B **48**, 13115 (1993).
[40]G. Kresse and J. Furthmüller, Phys. Rev. B **54**, 11169 (1996).
[41]G. Kresse and D. Joubert, Phys. Rev. B **59**, 1758 (1999).
[42]V. Potin, P. Ruterana, G. Nouet, R. C. Pond, and H. Morkoç, Phys. Rev. B **61**, 5587 (2000).
[43]F. Oba, H. Ohta, Y. Sato, H. Hosono, T. Yamamoto, and Y. Ikuhara, Phys. Rev. B **70**, 125415 (2004).
[44]Y. Hinuma, F. Oba, Y. Nose, and I. Tanaka, J. Appl. Phys. **114**, 043718 (2013).
[45]K. Momma and F. Izumi, J. Appl. Crystallogr. **44**, 1272 (2011).